Journal of ELECTRONIC MATERIALS, Vol. 48, No. 9, 2019
https://doi.org/10.1007/s11664-019-07327-y

Effect of TiO_2 Concentration on the Non-Volatile Memory Behavior of TiO_2-PVA Polymer Nanocomposites

JYOTI,[1] RAMNEEK KAUR,[2] SUKHDEEP SINGH,[3] JADAB SHARMA,[1] and S.K. TRIPATHI[1,3,4,5]

1.—Centre for Nanoscience and Nanotechnology, Panjab University, Chandigarh 160014, India. 2.—Department of Physics, Akal University, Talwandi Sabo, Punjab 151302, India. 3.—Department of Physics, Panjab University, Chandigarh 160014, India. 4.—e-mail: surya@pu.ac.in. 5.—e-mail: surya_tr@yahoo.com

In the current work, we report the fabrication of titanium dioxide polymer nanocomposite (TiO_2 PNC) memory devices. TiO_2 PNCs were fabricated at three different solution volume ratios with polymer polyvinyl alcohol (PVA), i.e. TiO_2-PVA :: 1:100, 1:50 and 1:10. The effect of increased concentration of TiO_2 nanoparticles (NPs) was studied. TiO_2 NPs were synthesized by the sol–gel method. High-resolution transmission electron microscopy images of the prepared TiO_2 NPs were acquired. Fluorine-doped tin oxide (FTO)-coated glass was used as a substrate for device fabrication. PNCs were characterized by x-ray diffraction spectroscopy, and the TiO_2-PVA (1:10) device was also morphologically characterized by field emission scanning electron microscopy. The thickness of the PNC film is 14 μm. These devices exhibit bipolar switching behavior, with the maximum ON/OFF current ratio (I_{ON}/I_{OFF}) of $\sim 10^3$ for the FTO/TiO_2-PVA (1:10)/Ag device. Current–voltage (I–V) curves show hysteresis as a result of the formation and rupture of conductive filaments due to the migration of oxygen vacancies. Write-read-erase-read test cycles show good repeatability, stability and retention properties. The results thus prove that the TiO_2-PVA devices are strong candidates for next-generation non-volatile memory devices because of their large ON/OFF current ratio, repeatability and stability.

Key words: Memory devices, ON/OFF current ratio, polymer nanocomposites, TiO_2 NPs

INTRODUCTION

Memory plays a vital role in storing or providing information in the many digital devices used in day-to-day life.[1–4] These devices have become an integral part of the modern lifestyle due to the increased dependence on portable electronic devices such as mobile phones, media players and personal data storage devices.[5]

All the current non-volatile memory devices are fabricated from inorganic materials that are based on charge storage and are used in complementary metal–oxide–semiconductor (MOS) processes.[6,7] In the case of inorganic materials, the fabrication of multiple active memory layers on a single Si wafer is limited by the technological challenges with single-crystal semiconductors. Feature size reduction of the memory devices is the only solution for improving the memory density of Si semiconductor devices. During this process, however, heat generation is a major problem. The other shortcomings in Si memory devices are slow programming, high operating voltage (10–20 V) and limited endurance.[8] In addition, a large amount of memory density is required to meet current consumer demand, which is a challenge with existing technology. In efforts to overcome these issues in conventional inorganic-based memory devices,

(Received February 1, 2019; accepted May 23, 2019; published online June 13, 2019)

organic-based memory devices are gaining in popularity.[9]

Organic electronics that include light-emitting diodes, non-volatile memory devices and solar cells have gained much attention due to their flexibility and ease of fabrication.[10–12] Among these, organic memory devices have recently been explored as a possible alternative to conventional semiconductor Si-based memory devices.[13,14] Extensive research has been carried out to develop organic memory devices that have a large ON/OFF current ratio (I_{ON}/I_{OFF}) and long retention time. In comparison to organic devices with metallic nanoparticles (NPs) in the active layer,[15,16] relatively little research has been focused on memory devices with semiconductor NPs in the active layer. Semiconductor NPs are now replacing the commonly used metal NPs (Ag, Cu and Au) as charge-trapping elements for electronic memory devices. Wang et al.[17] studied the memory effect of Cu-doped HfO_2 thin films, where the memory behavior was attributed to the formation of Cu conductive filaments.

Polymer nanocomposites (PNCs) have been studied extensively for the development of memory devices.[18–23] Kim et al.[24] reported that a polymer-NP blend layer could be used to improve the characteristics of the memory device. Also, PNC-based electronics offer simple and cheap electronic devices with the potential for low-temperature fabrication techniques, flexibility and wide area production. The way that information is stored in PNCs is completely different from that in silicon devices. In PNCs, the information is stored on the basis of high- and low-conductivity behavior with respect to applied voltage, whereas in silicon devices, the information is encoded in the form of "0" or "1" as the amount of data stored. In PNCs, the NPs act as the charge-storing elements in the polymer matrix. PNCs can be deposited on a variety of substrates, including glass, plastic, metal foils and wafers, by a number of techniques such as solution processing, spray-coating, spin-coating, dip-coating, roller-coating and ink-jet printing. Thus, much work is in progress for the development of PNC switching materials with desirable properties. Titanium dioxide (TiO_2) is among the most widely studied material because of its benefits such as low material and fabrication cost, simple preparation technology, eco-friendly nature, high dielectric constant and long-term stability. Polyvinyl alcohol (PVA) is a water-soluble polymer with a large number of hydroxyl groups. PVA serves as an insulating dielectric material in memory devices, and it also serves as a supporting layer. We chose PVA because of its high chemical and thermal resistance along with excellent electrical properties. PVA is studied extensively because of its benefits such as high solubility in water. Vishwanath et al.[25] studied an electrochemical-metallization-based resistive switching RAM device with a configuration of Al/TiO_2/Mo-doped In_2O_3, and investigated the resistive switching induced by formation and rupture of conductive filaments (FRCF) in the TiO_2 layer. Ge et al.[26] examined the switching modes in single-crystal TiO_2 memory devices. They have examined the effect of the concentration of oxygen vacancies (OVs) on the switching mechanism.

In this paper, we describe the performance of the bipolar resistive switching devices involving TiO_2 NPs embedded in PVA matrix at various concentrations. Research on TiO_2 NPs has been reported in the literature, but to the best of the authors' knowledge, as far as memory devices are concerned, no work has been reported on TiO_2 NPs embedded in polymer matrix. PVA stabilizes the TiO_2 NPs against agglomeration. Fluorine-doped tin oxide (FTO) glass was used as a substrate for device fabrication. The fabricated FTO/TiO_2-PVA/Ag devices (at different concentrations) exhibit bipolar switching, with the maximum I_{ON}/I_{OFF} of $\sim 5.08 \times 10^3$. The repeatability and stability of the FTO/TiO_2-PVA/Ag were confirmed by write–read–erase–read (WRER) cycles.

EXPERIMENTAL DETAILS

Synthesis of TiO_2 NPs

The chemicals utilized for synthesis of TiO_2 NPs were purchased from Sigma Aldrich. TiO_2 NPs were made by sol–gel method. Sixteen milliliters of titanium butoxide ($Ti(OC_4H_9)_4$) was dissolved in 8 mL of ethyl alcohol (C_2H_5OH) to make a colloidal solution. To this solution, a solution of concentrated H_2SO_4 and H_2O was added dropwise.[27] The mole ratio of $Ti(OC_4H_9)_4$:H_2O:C_2H_5OH was about 1.3:320.6:3.9. The above solution was maintained at 100°C for 30 min. The resulting solution was cooled naturally to room temperature and maintained there for a period of 7 days. The settled residue was filtered and dried at 100°C for 5 h. The dried gel was calcined at 550°C for 6 h to obtain the TiO_2 nanopowder.

Synthesis of the TiO_2-PVA PNCs

The solution of TiO_2 NPs (2 mg/mL) and PVA (5 mg/mL) was prepared separately in deionized (DI) water. For PNC synthesis, the as-prepared solutions of PVA (molecular weight $\sim$ 140,000) and TiO_2 NPs were mixed in different volume ratios (TiO_2: PVA:: 1:100, 1:50 and 1:10).

Device Fabrication

The device fabrication involved the following steps:

a Cleaning of the substrates: FTO glasses were used as the bottom electrode for fabricating the devices. FTO glasses were dipped in acetone and ultra-sonicated for 1 h to remove all impurities, followed by washing with distilled water.

b Deposition of the polymer nanocomposite layer: The drop-casting method was used to deposit

TiO_2-PVA PNC thin films, which served as an active layer for the memory device.

c Deposition of the top electrodes: In the present work, a silver electrode using silver paste was used as the top electrode for various electrical measurements. Figure 1 shows the schematic device architecture of the fabricated memory device.

Instrumentation

X-ray diffraction (XRD) diffractograms were recorded using a Rigaku MiniFlex 600 x-ray diffractometer with CuKα radiation in the 2θ range from 10° to 80°. High-resolution–transmission electron microscopy (HR-TEM) was acquired with a JEOL JEM-2100 electron microscope operated at a voltage of 200 kV. Field emission scanning electron microscopy (FE-SEM) was performed with a Hitachi SU-8000 (model: HI-0876-0003) operated at an accelerating voltage of 15 kV. For the characterization of the fabricated memory device, current–voltage (I–V) characteristic and WRER cycles were performed using a Keithley 6517A electrometer/high-resistance meter interfaced with a computer. All device measurements were performed at room temperature (300 K).

RESULTS AND DISCUSSION

Structural Characterization

The XRD spectrum of the TiO_2 NPs is depicted in Fig. 2a, which shows a highly crystalline nature with peaks corresponding to an anatase phase. Diffraction peaks corresponding to the (101), (004), (200), (105), (211), (204), (116), (220), and (215) planes are observed. These are indexed to the tetragonal anatase phase of the TiO_2 using PDF Card No. 841826 as reference. The Debye–Scherrer formula was used to calculate the crystallite size:[28]

$$D = \frac{k\lambda}{\beta \cos\theta} \quad (1)$$

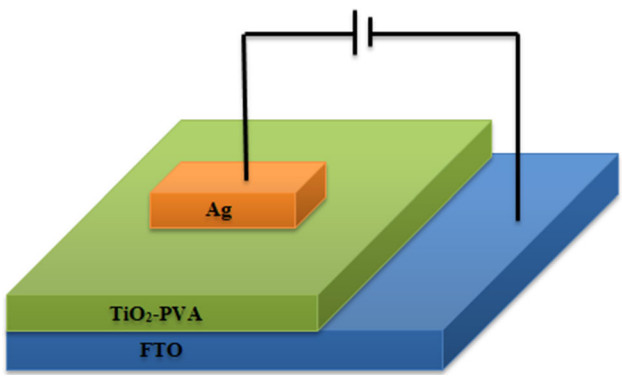

Fig. 1. Schematic device architecture of the fabricated memory devices.

where k is the Scherrer constant taken as unity, λ is the x-ray wavelength (1.54 Å), β is the full width at half maxima (FWHM) and θ is the diffraction angle. The most intense peak appears at 25.32° and is used to determine the crystallite size, which is found to be 20.7 nm. PVA shows a diffraction peak at around 20°. Figure 2b, c, and d shows the XRD spectra of the TiO_2-PVA polymer nanocomposite films at different volume ratios (1:100, 1:50 and 1:10, respectively). The XRD spectrum of the TiO_2-PVA (1:100) film shows a diffraction peak at 18.92°, which corresponds to the PVA polymer, and there is no peak corresponding to TiO_2 NPs, which indicates that the concentration of the TiO_2 NPs is very low and the film is amorphous in nature.[29] But as we increase the concentration of the TiO_2 NPs, the crystallinity of the films begin to increase. Reduced broadening of the diffraction profile was observed for the TiO_2-PVA (1:50) film, which was due to the increased concentration of TiO_2 NPs. It is also clear from the pattern in Fig. 2d that the crystallinity continues to increase with the further addition of TiO_2 NPs, and a peak at 25.32° appears, which is a characteristic peak corresponding to the tetragonal anatase phase of the TiO_2 NPs.[30] An HR-TEM nanograph of the prepared TiO_2 NPs is shown in Fig. 3. The size of the TiO_2 NPs is found to be $\sim$ 24 nm. Figure 4 shows the FE-SEM cross-sectional morphology of the TiO_2-PVA (1:10) layer. The FE-SEM micrograph shows that the film has a thickness of 14 μm.

Device Characterization

Figure 5 shows the I–V characteristics of the fabricated devices. For all devices, a forward bias is cycled as −5 V to 5 V and then in a reverse direction 5 V to −5 V. The charge stored in the device is directly proportional to the area under the hysteresis curve. In the fabricated devices, the current obtained in the second cycle was almost the same as that obtained in the first cycle, which indicates a negligible loss of the stored charge in the device further indicating that the device has very good stability and retention properties.

The FTO/TiO_2-PVA (1:100)/Ag device in Fig. 5a shows negligible hysteresis, which is due to the low charge storage capacity of the device. Thus, in order to improve the performance, the concentration of the TiO_2 NPs was increased in the PVA matrix. The FTO/TiO_2-PVA (1:50)/Ag and FTO/TiO_2-PVA (1:10)/Ag devices in Fig. 5b and c show that there is negligible current loss in the next cycle, which indicates the good endurance of the fabricated samples. Thus, with the increase in the concentration of TiO_2 NPs, the area under the hysteresis curve was found to increase, indicating the enhanced charge storage capability.

Various switching behavior mechanisms have been suggested, among which the conductive filament mechanism has been widely adopted. In this

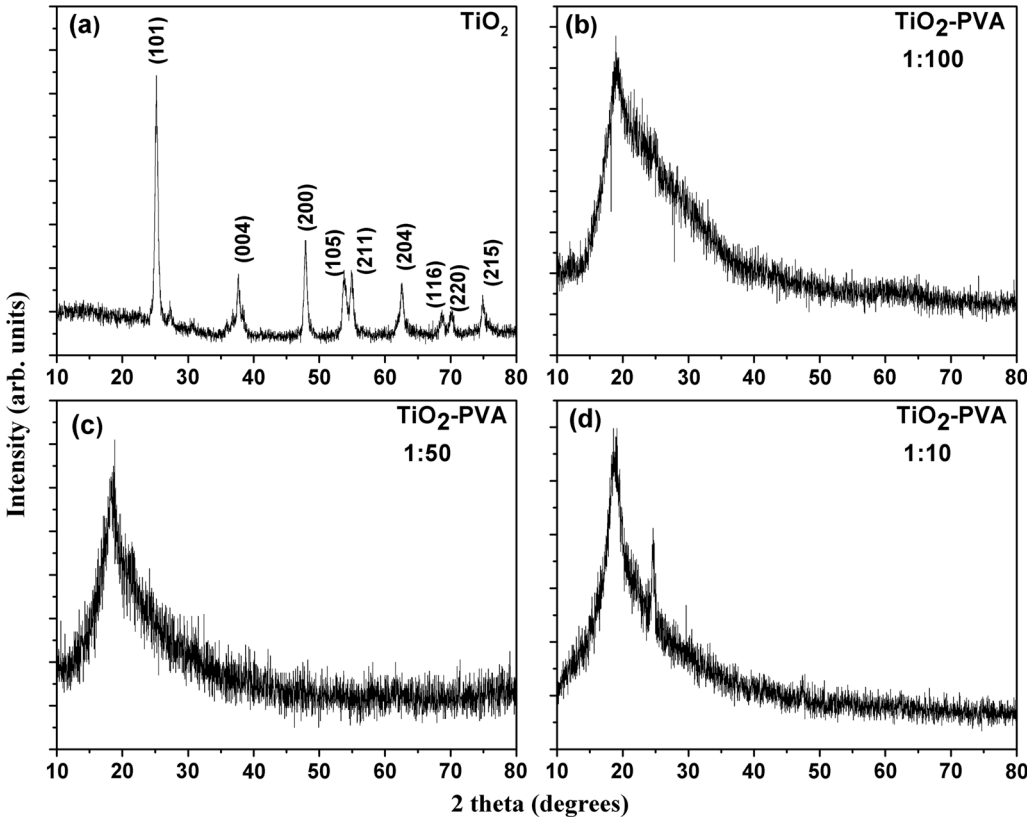

Fig. 2. XRD spectra of the (a) TiO_2 nanoparticles (b) TiO_2-PVA (1:100) (c) TiO_2-PVA (1:50) and (d) TiO_2-PVA (1:10).

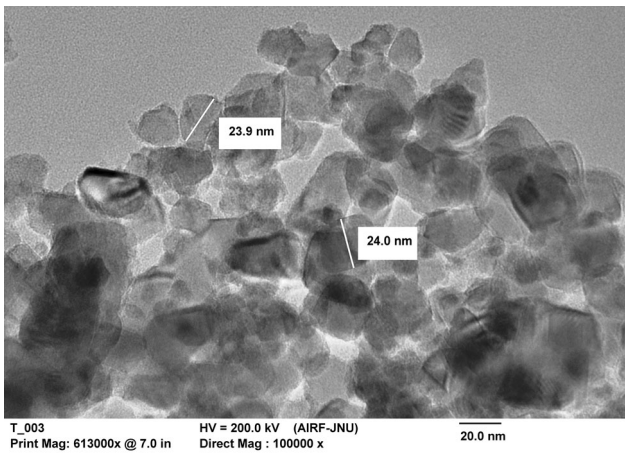

Fig. 3. HR-TEM nanograph of the TiO_2 NPs.

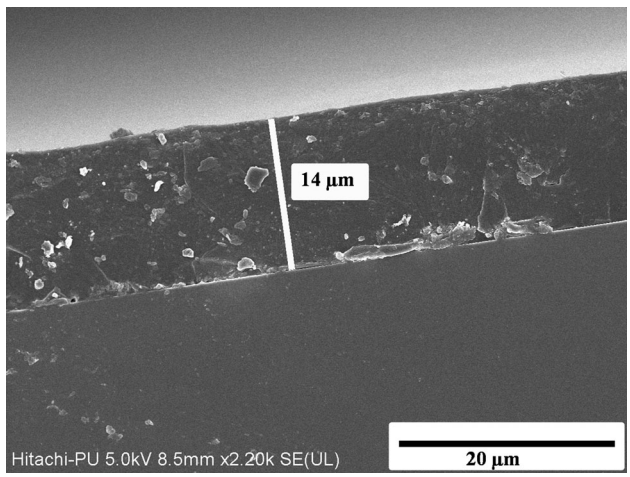

Fig. 4. FE-SEM cross-sectional morphology of TiO_2-PVA (1:10) layer.

mechanism, FRCF takes place in the active layer. Also, the existence of the OVs plays a major role in the switching of device by reduction and oxidation of the conductive filaments.[31,32] OVs are taken as the positive charge because they act like holes (i.e. the absence of electrons). As we apply the positive bias to the bottom electrode (FTO), OVs are repelled from the bottom electrode and move to the top electrode because of the positive charge of the hole. As we continue to increase the concentration of the TiO_2 NPs, more OVs are formed.[33,34] Thus a filamentary path is formed in the active layer which switches the device to a low-resistance state (LRS) from a high-resistance state (HRS). As we apply the negative bias, the bottom electrode attracts the OVs, which results in the transition from LRS to HRS due to the rupture of the conductive filament.[35,36] In the high-current region, thermal energy is generated due to the passage of high current through the conductive filament, which

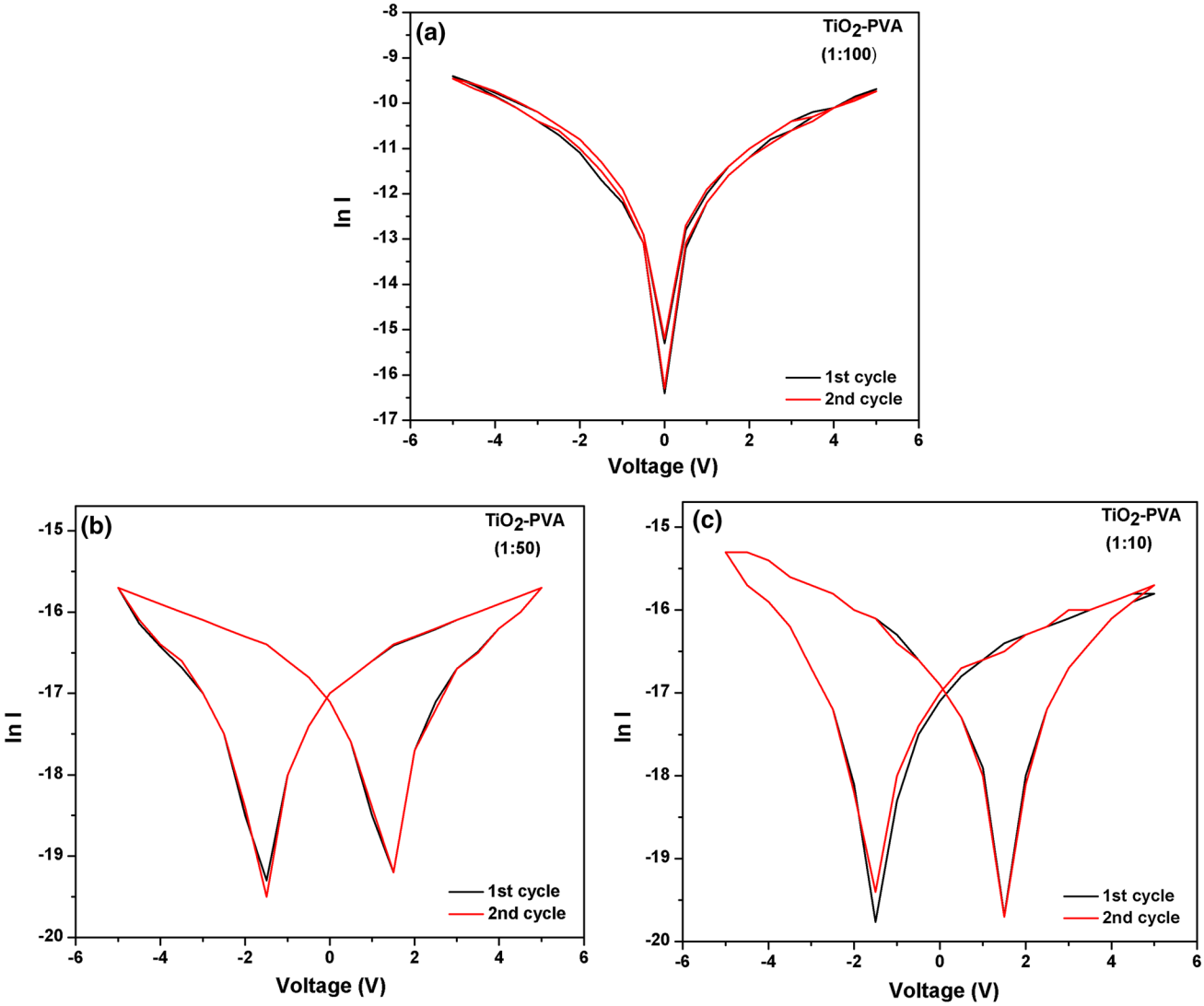

Fig. 5. Current–voltage characteristics of the fabricated memory devices (a) FTO/TiO_2-PVA (1:100)/Ag and (b) FTO/TiO_2-PVA (1:50)/Ag (c) FTO/TiO_2-PVA (1:10)/Ag.

further enhances the diffusion of the OVs. At the same time, the conductive filament shrinks and the current decreases. In this case, thermal diffusion dominates the migration of OVs. In the low-current region, less thermal energy is generated because of the passage of less current through the conductive filament, which increases the migration of OVs. Thus, in this case, the migration of OVs becomes dominant instead of thermal diffusion. The schematic diagram of the LRS and HRS in FTO/TiO_2-PVA/Ag devices is shown in Fig. 6. In the present work, the FRCF is very stable. Hence, it proves to be a very stable memory device with high endurance.

Memory performance of the devices has been verified by executing the WRER cycles. Figure 7 shows 10 WRER cycles executed for the fabricated memory devices. The input voltage levels applied for this purpose are 5 V, 2 V, −5 V, and 2 V for the operation of WRER, respectively. For any memory device, ON/OFF current ratio is the key parameter

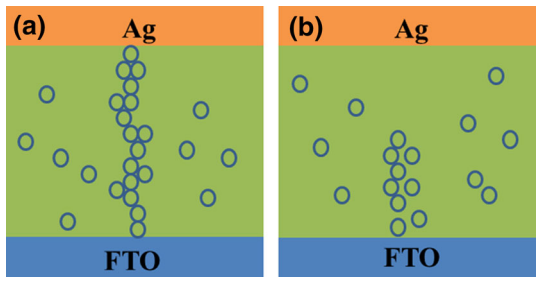

Fig. 6. Schematic diagram of LRS and HRS in FTO/TiO_2-PVA/Ag devices, respectively. The circles in (a) and (b) represent oxygen vacancies.

that decides the performance of the device. It is defined as the ratio of the current at the LRS and at HRS for the same applied voltage. In our work, the I_{ON}/I_{OFF} obtained for the fabricated devices, i.e. in the case of TiO_2-PVA(1:100), TiO_2-PVA (1:50) and TiO_2-PVA (1:10) is 1.089, 32.79, and 5.08×10^3,

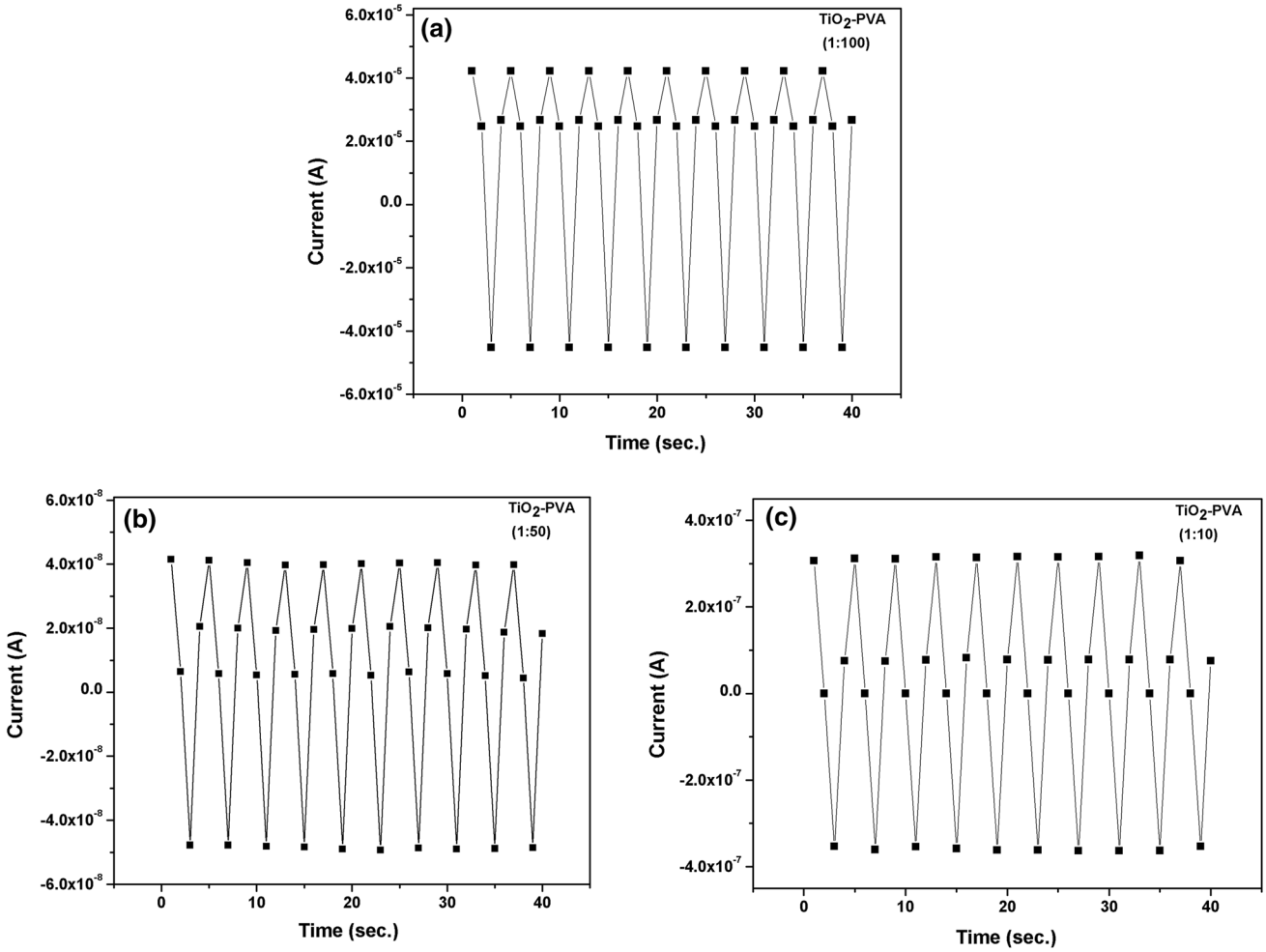

Fig. 7. WRER characteristics of the fabricated memory devices (a) FTO/TiO_2-PVA (1:100)/Ag, (b) FTO/TiO_2-PVA (1:50)/Ag and (c) FTO/TiO_2-PVA (1:10)/Ag.

Table I. I_{ON}/I_{OFF} of all the fabricated devices

Device	I_{ON}/I_{OFF}
FTO/TiO_2-PVA (1:100)/Ag	1
FTO/TiO_2-PVA (1:50)/Ag	33
FTO/TiO_2-PVA (1:10)/Ag	5×10^3

respectively, and are given in Table I. The trend of the I_{ON}/I_{OFF} is TiO_2-PVA (1:10) > TiO_2-PVA (1:50) > TiO_2-PVA (1:100). Thus, with the increase in TiO_2 NPs in the active layer of the memory devices, the I_{ON}/I_{OFF} increases. Also, the magnitude of the I_{ON}/I_{OFF} ratio reported for different devices is tabulated in Table II, where an I_{ON}/I_{OFF} of 10^2 was obtained for the Au/TiO_2/Pt device fabricated by Sahu et al.[37] Similarly, different I_{ON}/I_{OFF} ratios have been reported for other devices based on TiO_2 NPs.[38–41] However, in the present work, a maximum I_{ON}/I_{OFF} ratio of 5.08×10^3 was obtained for the FTO/TiO_2-PVA (1:10)/Ag device.

Endurance characteristics of a memory device are represented by the number of cycles for which it

Table II. I_{ON}/I_{OFF} of the various TiO_2 devices

Device	I_{ON}/I_{OFF}	References
Au/TiO_2/Pt	10^2	37
Cu/TiO_2(nanotube)/Ti	14	38
Pt/PAA/TiO_2(nanotube)/Ti	5	39
Al/TiO_2 nanowires/Ti	70	40
Ag/TiO_2/Ti	27	41
FTO/TiO_2-PVA (1:10)Ag	5.08×10^3	This work

shows steady ON- and OFF-state levels without degradation. Figure 8 depicts the endurance characteristics of the fabricated devices, which show steady ON- and OFF-state levels with almost no degradation for 10 cycles. This indicates that the devices have good endurance capability.

CONCLUSION

TiO_2 NPs have been successfully synthesized by the sol–gel method. The XRD pattern of the TiO_2 NPs reveals a tetragonal anatase phase with

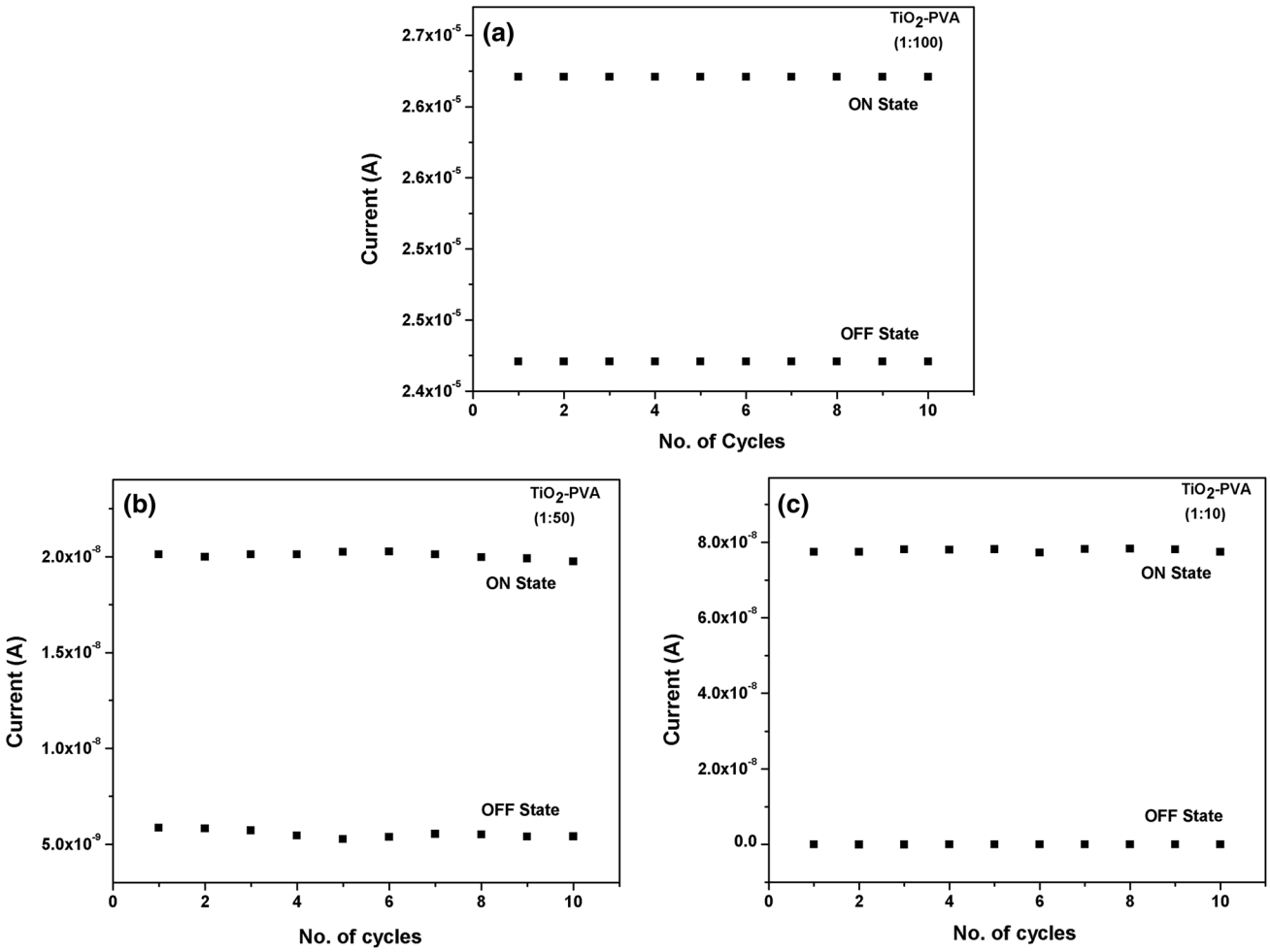

Fig. 8. Endurance characteristics of the fabricated memory devices (a) FTO/TiO_2-PVA (1:100)/Ag, (b) FTO/TiO_2-PVA (1:50)/Ag and (c) FTO/TiO_2-PVA (1:10)/Ag.

crystallite size of 20.7 nm. The crystalline behavior of the films increases with increased TiO_2 NP concentration in the PVA matrix. The cross-sectional morphology was probed using FE-SEM, and the thickness of the film was found to be 14 μm. The particle size of the TiO_2 NPs, from HR-TEM images, was found to be $\sim$ 24 nm. From the current–voltage characteristics of the fabricated memory devices, it was concluded that the device performance improves with increased concentration of TiO_2 NPs in the PVA matrix. On the basis of FRCF made by OVs, the switching mechanism is explained. The TiO_2-PVA (1:10) device shows good stability and endurance, and exhibits the maximum I_{ON}/I_{OFF} $\sim 10^3$. This is because increased concentration of TiO_2 NPs enhances the migration of OVs and leads to the formation of stable conductive filaments. Therefore, from the work carried out, we can conclude that the TiO_2-PVA PNCs are strong candidates for memory storage applications.

ACKNOWLEDGMENTS

This work is financially supported by the DST (PURSE) and CAS Grant. Ms. Jyoti is grateful to DST, New Delhi for provision of the fellowship.

REFERENCES

1. G.U. Siddiqui, M.M. Rehman, and K.H. Choi, *Polym. J.* 100, 102 (2016).
2. S. Goswami, A.J. Matula, S.P. Rath, S. Hedstrion, S. Saha, M. Annamalai, D. Sengupta, A. Patra, S. Gosh, H. Jani, S. Sarkar, M.R. Mothapothula, C.A. Nijhuis, J. Martin, S. Goswami, V.S. Batista, and T. Venkatensan, *Nat. Mater.* 16, 1216 (2017).
3. R. Kaur and S.K. Tripathi, *Org. Electron.* 61, 235 (2018).
4. P.F. Lee and J.Y. Dai, *Nanotechnology* 21, 295706 (2010).
5. S.K. Tripathi, R. Kaur, and Jyoti, *Mater. Sci. Eng. B* 211, 7 (2016).
6. H. Yu, C.C. Chung, N. Shewmon, S. Ho, J.H. Carpenter, R. Harrabee, T. Sun, J.L. Jones, H. Ade, B.T. O'Connor, and F. So, *Adv. Funct. Mater.* 27, 1700461 (2017).
7. D. Liu, Q. Lin, Z. Zang, M. Wang, P. Wangyang, X. Tang, M. Zhou, and W. Hu, *ACS Appl. Mater. Interfaces* 9, 6171 (2017).

8. F. Pan, C. Chen, Z.S. Wang, Y. Yang, J. Yang, and F. Zeng, *Prog. Nat. Sci. Mater.* 20, 01 (2010).
9. R. Kaur and S.K. Tripathi, *Microelectron. Eng.* 133, 59 (2015).
10. A. Kuzmich, D. Padula, H. Ma, and A. Troisi, *Energy Environ. Sci.* 10, 395 (2017).
11. M. Gutiérrez, C. Martin, K. Kennes, J. Hofkens, M.V. Auweraer, F. Sánchez, and A. Douhal, *Adv. Opt. Mater.* 6, 1701060 (2018).
12. R. Kaur, J. Kaur, and S.K. Tripathi, *Solid State Electron.* 109, 82 (2015).
13. C.C. Shih, W.Y. Lee, and W.C. Chen, *Mater. Horiz.* 3, 294 (2016).
14. Y.H. Chou, Y.C. Chiu, W.Y. Lee, and W.C. Chen, *Chem. Commun.* 51, 2562 (2015).
15. Y. Zhou, L. Zhou, Y. Yan, S.T. Han, J. Zhuang, Q.J. Sun, S.T. Han, and V.A.L. Roy, *J. Mater. Chem. C.* 5, 8415 (2017).
16. P.C. Kao, C.C. Liu, and T.Y. Li, *Org. Electron.* 12, 203 (2015).
17. Y. Wang, Q. Liu, S. Long, W. Wang, Q. Wang, M. Zhang, S. Zhang, Y. Li, Q. Lou, J. Yang, and M. Liu, *Nanotechnology* 21, 045202 (2010).
18. P. Zang, C. Gao, B. Xu, C. Jiang, M. Gao, and D. Xue, *Small* 12, 2077 (2016).
19. M.M. Rehman, B.S. Yang, Y.J. Yang, K.S. Karimov, and K.H. Choi, *Curr. Appl. Phys.* 17, 533 (2017).
20. D. Chaudhary, S. Munjal, N. Khare, and V.D. Vankar, *Carbon* 130, 553 (2018).
21. R.M. Mutiso and K.I. Winey, *Prog. Polym. Sci.* 40, 63 (2015).
22. G. Khurana, P. Misra, and R.S. Katiyar, *Carbon* 76, 341 (2014).
23. R. Kaur, J. Singh, and S.K. Tripathi, *Curr. Appl. Phys.* 17, 756 (2017).
24. J.M. Kim, D.H. Lee, J.H. Jeun, T.S. Yoon, H.H. Lee, J.W. Lee, and Y.S. Kim, *Synth. Met.* 161, 1155 (2011).
25. S.K. Vishwanath and J. Kim, *J. Mater. Chem. C* 4, 10967 (2011).
26. J. Ge, M. Chaker, and A.C.S. Appl, *Mater. Interfaces* 9, 16327 (2017).
27. S.K. Tripathi, M. Rani, and N. Singh, *Electrochem. Acta* 167, 179 (2015).
28. M.M.E. Nahass, H.S. Soliman, and A. El, Denglawey. *Appl. Phys. A* 122, 775 (2016).
29. A.C. Khot, N.D. Desai, K.V. Khot, M.M. Salunkhe, M.A. Chougule, T.M. Bhave, R.K. Kamat, K.P. Musselman, and T.D. Dongale, *Mater. Des.* 151, 37 (2018).
30. C.C. Yang, *J. Membr. Sci.* 288, 51 (2007).
31. N. Raghavan, M. Bosman, D.D. Frey, and K.L. Pey, *Microelectron. Reliab.* 54, 2266 (2014).
32. H.H. Pham and L.W. Wang, *Phys. Chem. Chem. Phys.* 17, 541 (2015).
33. K. Park and J.S. Lee, *RSC Adv.* 6, 21736 (2016).
34. S. Nigo, M. Kubota, Y. Harada, T. Hirayama, S. Kato, H. Kitazawa, and G. Kido, *J. Appl. Phys.* 112, 033711 (2012).
35. W. Hu, L. Zou, R. Chen, W. Xie, X. Chen, N. Qin, S. Li, G. Yang, and D. Bao, *Appl. Phys. Lett.* 104, 143502 (2014).
36. M. Janousch, G.I. Meijer, U. Staub, B. Delly, S.F. Karg, and B.P. Andreasson, *Adv. Mater.* 19, 2332 (2007).
37. V.K. Sahu, A.K. Das, R.S. Ajimsha, and P. Misra, *J. Phys. D Appl. Phys.* 21, 215101 (2018).
38. D. Conti, A. Lamberti, S. Porro, P. Rivolo, A. Chiolerio, C.F. Pirri, and C. Ricciardi, *Nanotechnology* 27, 485208 (2016).
39. D. Chu, A. Younis, and S. Lio, *J. Phys. D Appl. Phys.* 45, 355306 (2012).
40. J.E. Yoo, K. Lee, A. Tighineanu, and P. Schmuki, *Electrochem. Commun.* 34, 177–180 (2013).
41. F. Yang, S. Mao, S. Zhu, Y. Jia, L. Yuan, M. Salmen, and B. Sun, *Chem. Phys. Lett.* 706, 477 (2018).